

Volcanology and eruptive histories of the Erongo Volcanic Complex and the Paresis Igneous Complex, Namibia: implications for mineral deposit styles

Franco Pirajno¹, David Phillips² and Richard A. Armstrong²

¹Geological Survey of Western Australia, 100 Plain Street, East Perth WA 6004, Australia

²Research School of Earth Sciences, The Australian National University, Canberra ACT 0200, Australia

The Erongo Volcanic Complex and the Paresis Igneous Complex belong to the dominantly Early Cretaceous Damaraland alkaline province, Namibia. They are well-preserved volcanic centres characterised by explosive activity but have contrasting eruptive styles. These eruptive styles reflect the diverse nature of the parent magmas, depth of magma chambers and consequently different types of associated hydrothermal activity. We present new age determinations for both the Erongo and Paresis complexes. New U-Pb SHRIMP dating of zircons and step-heating ⁴⁰Ar/³⁹Ar of K-feldspar indicate eruption ages in the range of 135-132 Ma for both complexes.

The evolutionary sequence of the Erongo Volcanic Complex began with the outpouring of basaltic lavas, followed by voluminous eruptions of rhyodacitic ignimbrites from a central vent. Granitic magma was later emplaced in a ring structure from which rhyolitic, high-temperature rheoignimbrites were erupted. This granite caused widespread boron and fluorine metasomatism and resulted in structurally controlled, greisen-style tungsten and tin mineralisation.

The sequence of events that led to the emplacement of the Paresis Igneous Complex is more complex as it involved several episodes of effusive and intrusive activity. The magmatic products have alkaline to peralkaline compositions. The Paresis explosive activity is characterised by comenditic and rhyolitic ignimbrites and debris flows. The nature of these volcanoclastic deposits suggests substantial interaction with water. Evidence of hydrothermal activity can be seen in a deeply eroded and extensively fractured area where rock types are silicified and altered to an assemblage of quartz-sericite-pyrite. Although no mineralisation is at present known in the Paresis Igneous Complex, metalliferous deposits of alkaline porphyry-epithermal style may exist.

Introduction

Intracontinental anorogenic and alkaline magmatism is widespread in southwestern Africa (Fig. 1). In Namibia, alkaline complexes include plugs, pipes, dykes, subvolcanic intrusions and large ring complexes (Pirajno, 1994). The Namibian complexes are distributed in well-defined provinces that tend to be aligned along east-northeast trends that are probably related to pre-existing crustal zones of weakness (Fig. 1). Three main provinces are recognised: the Early Cretaceous (138-124 Ma) Damaraland Alkaline Province; Watkins *et al.*, 1994, Milner *et al.* 1995); the Lüderitz Alkaline Province also of Early Cretaceous age and the Tertiary Auas Province. A fourth province includes igneous complexes and carbonatites of the Kuboos-Bremem line but this is of late Pan-African age (ca 490-550 Ma; Smithies and Marsh, 1998).

In this contribution we focus on two of the best preserved volcanic systems in Southern Africa: the *Erongo Volcanic Complex* and the *Paresis Igneous Complex*, both of which are part of the Damaraland province. In addition, we report new age determinations obtained from U-Pb SHRIMP analyses of zircons and ⁴⁰Ar/³⁹Ar step-heating analyses on K-feldspars. The former is the largest of the Namibian anorogenic complexes and consists of a volcano-plutonic caldera structure characterised by a succession of tholeiitic lavas, thick rhyodacitic ash-flow tuffs and a ring dyke of tourmaline-rich granite (Erongo Granite) with associated Sn, W and U mineralisation (Pirajno and Schlögl, 1987; Pirajno, 1990). The Paresis Igneous Complex is markedly different and is characterised by alkaline to peralkaline intrusive, effusive and volcanoclastic rocks. The effusive rocks are comendite, rhyolitic ignimbrites and volcanoclastic rocks that include debris-flows (Siedner,

1965a and b). The nature of the volcanoclastic deposits suggest substantial interaction with water. Evidence of hydrothermal activity can be seen in a deeply eroded, extensively fractured area where rock types are silicified and hydrothermally altered to an assemblage of quartz-sericite-pyrite (Pirajno *et al.*, 1990). Although no mineralisation is at present known in the Paresis Igneous Complex, the potential for metalliferous deposits of alkaline porphyry-epithermal style exists.

Overview of the Damaraland province

The Damaraland province is the largest and best known of the Namibian alkaline provinces and is also important from the point of view of mineral resources (Pirajno, 1994). The province extends northeastwards for approximately 350 km from the Atlantic coast (Fig. 1). It contains at least 21 complexes, ranging from granitic, layered basic complexes, carbonatite to peralkaline types. A comprehensive analysis of the geochemical evolution of the Damaraland province was conducted by Prins (1981). Recent age determinations, based on Rb-Sr and ⁴⁰Ar/³⁹Ar systems, indicate that the Damaraland complexes were emplaced during the Early Cretaceous, between 138 and 124 Ma (Milner *et al.*, 1995). The igneous complexes of the Damaraland province are closely associated with the continental flood basalts of the Paraná-Etendeka Province, the opening of the South Atlantic Ocean and may be linked to the Tristan da Cunha mantle plume (Ewart *et al.*, 1998a and b).

Apart from the Erongo and Paresis complexes discussed in this paper, some of the other, and perhaps better known, Damaraland alkaline complexes include the Messum Igneous Complex (Ewart *et al.*, 1998a and b), Okenyenya (Watkins *et al.*, 1994) and the Brandberg al-

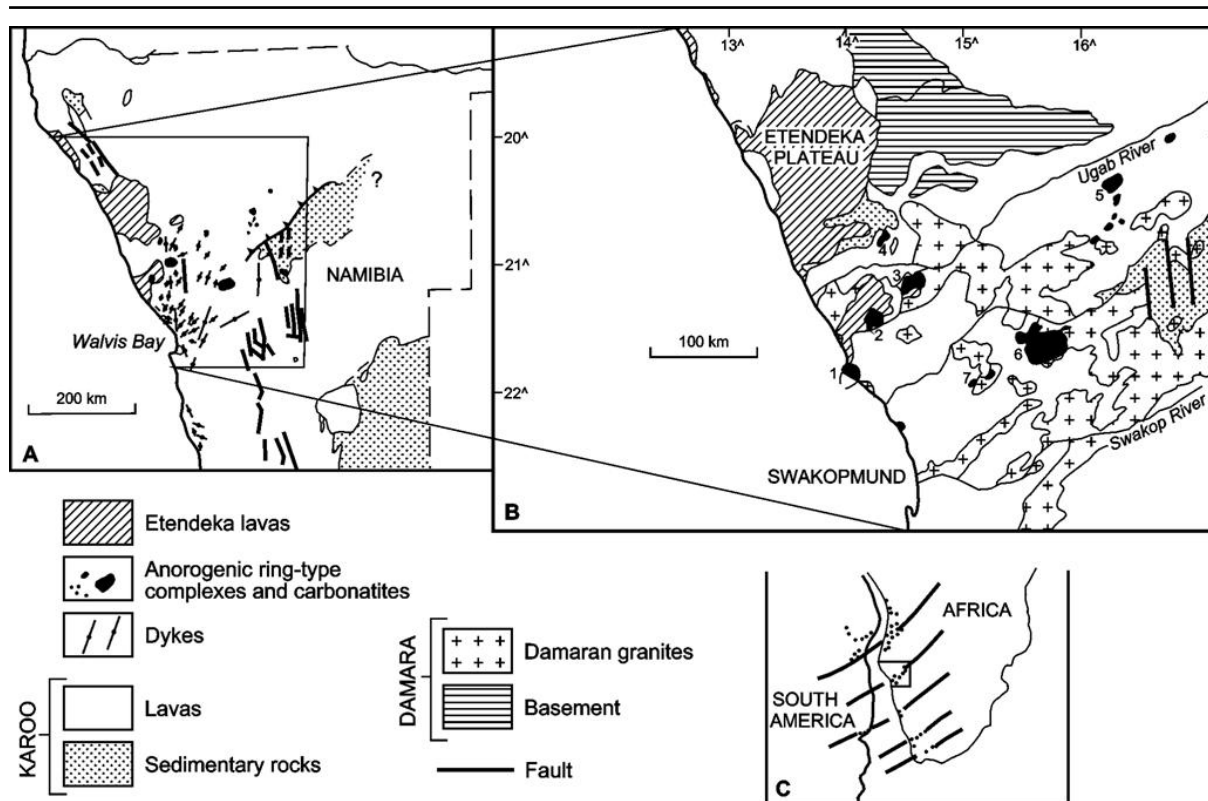


Figure 1: (A) Schematic illustration showing distribution of Etendeka and Karoo continental flood basalts and associated dyke swarms in north-central Namibia; (B) Distribution of Etendeka lavas and associated anorogenic ring-type alkaline complexes and carbonatites; numbered complexes are 1) Cape Cross, 2) Messum, 3) Brandberg, 4) Doros, 5) Paresis, 6) Erongo and 7) Spitzkop; (C) Relationship of alkaline complexes in southwestern Africa and the east coast of South America to transform directions (after Marsh, 1973).

kaline complex (Diehl, 1990). The Otjohorongo granitic ring complex (Miller, 1980), for which we report a new $^{40}\text{Ar}-^{39}\text{Ar}$ age, is the least known of the complexes.

In addition to the above-mentioned ring complexes, at least six carbonatite complexes belong to the Damaraland province (Pirajno, 1994). They are Okorusu, Kalkfeld, Ondurakorume, Osongombo, Kwaggspan and Otjisazu. Of these, Okorusu is formed by a number of concentric intrusions of carbonatite, syenite, foyaite, ijilite and tinguaitite. The metasedimentary country rocks are strongly fenitized around the carbonatite and are also mineralised with fluorite.

U-Pb and $^{40}\text{Ar}-^{39}\text{Ar}$ geochronology

Age determinations were carried out on mineral separates (zircons and K-feldspars) from the Erongo Volcanic Complex, the Paresis Igneous Complex and, for comparative purposes, the Otjohorongo ring complex, using U-Pb SHRIMP and $^{40}\text{Ar}/^{39}\text{Ar}$ step-heating methods. Analytical procedures are given in Appendix 1.

U-Pb Results

Paresis Complex quartz-feldspar porphyry

The zircons from this quartz-feldspar porphyry are clear and euhedral with the well developed composi-

tional zoning which is typical of crystallisation in a felsic magma. A few rounded cores were observed but these were avoided during analysis.

Fifteen U-Pb analyses were performed on different zircons and the data are listed in Table 1, and plotted on a Tera-Wasserburg U-Pb concordia diagram (Fig. 2A). The data are plotted by convention as measured ratios, i.e. uncorrected for common Pb, and the data lie on a mixing line between the radiogenic Pb composition (on the concordia) and a common Pb component. The effects of recent Pb-loss are seen as a shift of the data points to the right. The analyses, plotted as filled circles, all conform to a single population giving a weighted mean $^{206}\text{Pb}/^{238}\text{U}$ age of 134.3 ± 1.7 Ma ($n=14$; MSWD = 0.77; probability = 0.69). A single analysis (5.1) falls outside this group, giving an older apparent $^{206}\text{Pb}/^{238}\text{U}$ age and may indicate the presence of an older, inherited component.

Erongo Volcanic Complex, Ombu Ash Flow Tuff (OAF)

The zircons from this tuff are variable in form and comprise fragments and whole subhedral grains. Cathodoluminescence imaging reveals well developed magmatic compositional and occasional sector zoning, as well as structured grains with rounded cores and magmatic overgrowths.

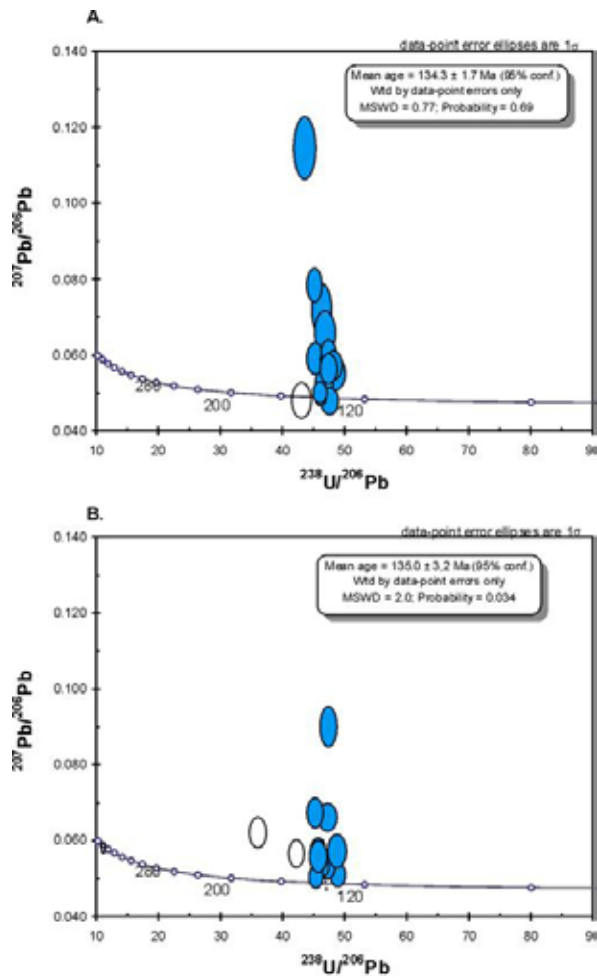


Figure 2: Concordia diagrams for samples of (A) quartz-feldspar porphyry (Paresis Igneous Complex) and (B) Ombu Ash Flow Tuff (Erongo Volcanic Complex).

In contrast to the quartz-feldspar porphyry sample, the U-Pb SHRIMP analyses on zircons from the OAF T sample of the Erongo Complex show a complex and heterogeneous age population comprising a mixture of a magmatic population and a variable age population of xenocrystic zircons. Within the presumed magmatic population there is also some scatter which might be a consequence of Pb-loss but the best estimate of an age of emplacement for this tuff is obtained by calculating a weighted mean ²⁰⁶Pb/²³⁸U age for the 10 analyses plotted in Figure 2B. This ²⁰⁶Pb/²³⁸U age is 135.0 ± 3.2 Ma (MSWD = 2.0; probability = 0.034). The six analyses which do not plot within this group are clearly older and are interpreted as xenocrysts either inherited from the source or picked up during eruption/emplacement. This commonly observed phenomenon emphasises the problems which are inherent in dating tuffs using multi-grain conventional techniques as the xenocrysts are in many cases discrete whole grains, and not cores, making identification difficult even with cathodoluminescence imaging. Apparent ages of the xenocrysts include known basement ages in the region (circa 2100, 1000 and 580 Ma) as well as some evidence of Jurassic and younger ages.

New ⁴⁰Ar/³⁹Ar analytical results (Table 2, Fig. 3) are reported for K-feldspar separates from a quartz-feldspar porphyry in the Paresis Igneous Complex and a granite porphyry in the Otjohorong Complex. Although the latter complex is not described in the present study, the data are included for comparative purposes. The K-feldspar separate from the Paresis Igneous Complex porphyry was step-heated in 18 increments and yields a plateau age of 130.6 ± 1.0 Ma (2σ). ⁴⁰Ar/³⁹Ar step-heating analyses of the K-feldspar separate from the Otjohorong granite porphyry produced a very similar age spectrum, with a plateau age of 131.6 ± 0.8 Ma (2σ). These data are indistinguishable from laser step-heating results reported for mineral separates from various Etendeka volcanic units by Renne *et al.* (1996). These authors recorded plateau dates on plagioclase, hornblende and biotite ranging from 129.3 ± 0.7 Ma to

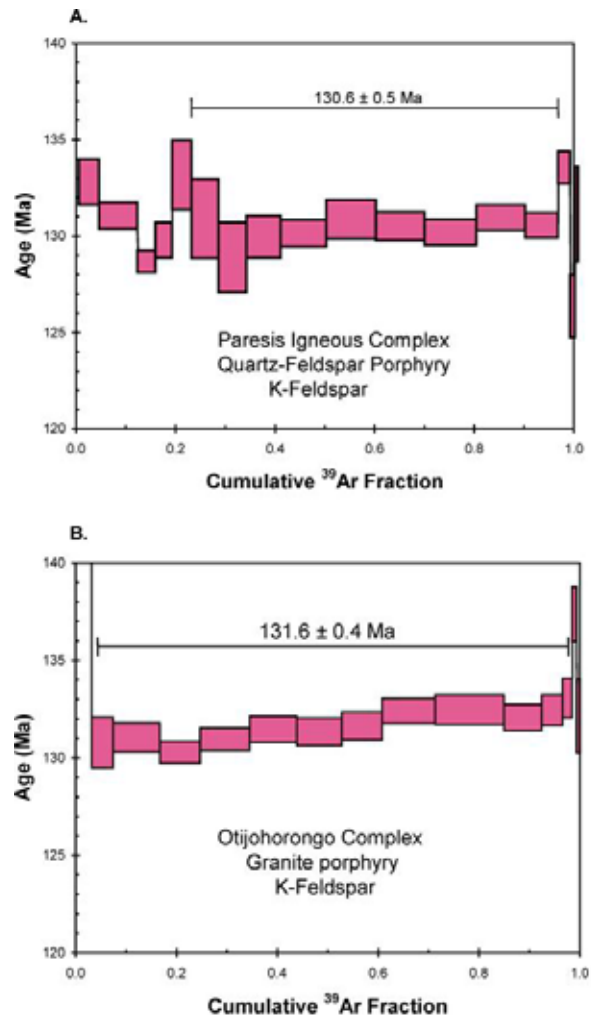


Figure 3: ⁴⁰Ar/³⁹Ar apparent age spectra for K-feldspar separates from (A) quartz-feldspar porphyry (Paresis Igneous Complex) and (B) granite porphyry (Otjohorong Complex). Age error bars are one standard deviation and exclude the uncertainties in the J-value. The age plateau is indicated by the horizontal line and its uncertainty includes the error in the J-value, but excludes the uncertainty in the age of the fluence monitor, GA1550.

Table 1 : Summary of SHRIMP U-Pb zircon results

Grain .spot	U ppm	Th ppm	Th/U	Pb* ppm	$\frac{^{206}\text{Pb}}{^{208}\text{Pb}}$	f ₂₀₆ %	Radiogenic Ratios				Ages (in Ma)										
							$\frac{^{206}\text{Pb}}{^{238}\text{U}}$	\pm	$\frac{^{207}\text{Pb}}{^{235}\text{U}}$	\pm	$\frac{^{206}\text{Pb}}{^{238}\text{U}}$	\pm	$\frac{^{207}\text{Pb}}{^{235}\text{U}}$	\pm							
Pareisis Complex; QFP																					
1.1	95	35	0.4	2	0.002612	2.97	0.0209	0.0006	0.0006	133.2	3.8	133.2	3.8								
2.1	107	73	0.7	2	0.002783	0.85	0.0204	0.0006	0.0006	130.2	3.7	130.2	3.7								
3.1	62	42	0.7	1	0.001425	2.19	0.0208	0.0006	0.0006	132.7	3.9	132.7	3.9								
4.1	119	56	0.5	3	0.000010	0.53	0.0212	0.0005	0.0005	135.4	3.4	135.4	3.4								
5.1*	59	39	0.6	2	0.001852	<0.1	0.0231	0.0007	0.0007	147.5	4.4	147.5	4.4								
6.1	107	70	0.7	3	0.000958	1.33	0.0217	0.0005	0.0005	138.5	3.3	138.5	3.3								
7.1	236	227	1	6	0.000193	1.30	0.0207	0.0005	0.0005	132.2	3.1	132.2	3.1								
8.1	216	127	0.6	5	0.000010	1.55	0.0207	0.0004	0.0004	132.1	2.7	132.1	2.7								
9.1	55	45	0.8	1	0.000010	8.30	0.0210	0.0007	0.0007	133.7	4.6	133.7	4.6								
10.1	127	59	0.5	3	0.000598	3.77	0.0212	0.0005	0.0005	135.5	3.1	135.5	3.1								
11.1	117	59	0.5	3	0.001505	<0.1	0.0209	0.0005	0.0005	133.6	3.1	133.6	3.1								
12.1	395	196	0.5	9	0.000051	0.10	0.0216	0.0004	0.0004	137.7	2.4	137.7	2.4								
13.1	229	104	0.5	5	0.000356	0.22	0.0216	0.0004	0.0004	137.8	2.8	137.8	2.8								
14.1	172	72	0.4	4	0.000302	1.11	0.0204	0.0005	0.0005	130.4	3.1	130.4	3.1								
15.1	179	84	0.5	4	0.000010	1.00	0.0208	0.0005	0.0005	132.7	3.1	132.7	3.1								
Erongo Complex; OAFI																					
1.1*	184	37	0.2	30	0.000153	0.245	0.1694	0.0032	0.0032	1.674	0.047	0.0717	0.0013	1009	18	999	18	977	37		
3.2	163	111	0.68	4	0.000010	0.17	0.0205	0.0005	0.0005	0.4005	0.0148	0.1316	0.0057	130.5	2.8	130.5	2.8	2145	56	2119	79
4.1*	203	117	0.6	92	0.000010	0.016	0.4005	0.0148	0.0148	7.266	0.440	0.1316	0.0057	2171	68	2145	56	1725	82	1996	155
4.2*	214	142	0.66	64	0.000122	0.227	0.2639	0.0099	0.0099	4.465	0.424	0.1227	0.0102	1510	51	1725	82	1996	155		
8.2	158	100	0.6	4	0.000040	0.99	0.0217	0.0005	0.0005	0.0217	0.0005	0.0217	0.0005	138.5	3.1	138.5	3.1	2.8	2.8	2.8	2.8
9.2	185	121	0.7	4	0.000694	0.40	0.0212	0.0004	0.0004	0.0212	0.0004	0.0212	0.0004	135.2	2.8	135.2	2.8	3.0	3.0	3.0	3.0
10.1	193	127	0.7	5	0.001133	0.41	0.0216	0.0005	0.0005	0.0216	0.0005	0.0216	0.0005	137.9	3.0	137.9	3.0	11	11	11	11
11.1*	175	73	0.42	17	0.000019	<0.1	0.0950	0.0018	0.0018	0.0950	0.0018	0.0950	0.0018	585	11	585	11	3.0	3.0	3.0	3.0
12.1	167	124	0.75	4	0.001223	0.11	0.0221	0.0005	0.0005	0.0221	0.0005	0.0221	0.0005	140.8	3.0	140.8	3.0	3.5	3.5	3.5	3.5
13.1	129	399	3.1	3	0.002572	2.11	0.0208	0.0006	0.0006	0.0208	0.0006	0.0208	0.0006	132.6	3.5	132.6	3.5	5.5	5.5	5.5	5.5
14.1*	303	279	0.9	10	0.000852	1.60	0.0275	0.0009	0.0009	0.0275	0.0009	0.0275	0.0009	175.1	5.5	175.1	5.5	3.6	3.6	3.6	3.6
15.1*	147	129	0.9	4	0.002717	0.88	0.0236	0.0006	0.0006	0.0236	0.0006	0.0236	0.0006	150.2	3.6	150.2	3.6	3.1	3.1	3.1	3.1
16.1	173	154	0.9	4	0.003277	5.17	0.0201	0.0005	0.0005	0.0201	0.0005	0.0201	0.0005	128.1	3.1	128.1	3.1	3.4	3.4	3.4	3.4
17.1	122	130	1.1	3	0.000027	2.27	0.0204	0.0005	0.0005	0.0204	0.0005	0.0204	0.0005	138.4	3.3	138.4	3.3	3.3	3.3	3.3	3.3
18.1	89	82	0.9	2	0.002864	0.97	0.0204	0.0005	0.0005	0.0204	0.0005	0.0204	0.0005	130.0	3.3	130.0	3.3	3.6	3.6	3.6	3.6
19.1	101	52	0.5	2	0.000321	0.78	0.0218	0.0006	0.0006	0.0218	0.0006	0.0218	0.0006	138.7	3.6	138.7	3.6				

Notes : (1) Uncertainties given at the one σ level; (2) f₂₀₆% denotes the percentage of ²⁰⁶Pb that is common Pb.
 (3) * analysis not included in weighted mean age calculation

Table 2: $^{40}\text{Ar}/^{39}\text{Ar}$ analytical data for K-feldspar samples from the Paresis quartz-feldspar porphyry and the Otjohorong granite porphyry

Step No	T(°C)	$^{36}\text{Ar}/^{39}\text{Ar}$	$^{37}\text{Ar}/^{39}\text{Ar}$	$^{40}\text{Ar}/^{39}\text{Ar}$	% $^{40}\text{Ar}^*$	$^{40}\text{Ar}^*/^{39}\text{Ar}$	Cum% ^{39}Ar	Age (Ma)	± I.S.D.
PA 158 K-Feldspar; Paresis quartz-feldspar porphyry; 1.41 mg; J = 0.008414 ± 0.000025									
1	650	0.0247	0.0329	16.423	55.3	9.088	3.94	132.9	1.2
2	750	0.0092	0.0400	11.740	76.3	8.964	11.59	131.2	0.7
3	800	0.0091	0.0158	11.519	76.4	8.796	15.19	128.8	0.6
4	850	0.0190	0.0091	14.542	61.1	8.873	18.72	129.9	0.9
5	900	0.0178	0.0089	14.443	63.2	9.114	22.36	133.3	1.8
6	950	0.0243	0.0069	16.175	55.3	8.953	27.76	131.1	2.1
7	975	0.0235	0.0062	15.804	55.8	8.811	33.51	129.1	1.8
8	1000	0.0214	0.0069	15.256	58.2	8.886	40.17	130.1	1.1
9	1025	0.0187	0.0087	14.478	61.5	8.899	49.34	130.3	0.7
10	1050	0.0156	0.0130	13.619	65.7	8.952	59.23	131.1	1.0
11	1075	0.0136	0.0145	13.000	68.7	8.926	69.04	130.6	0.7
12	1100	0.0134	0.0111	12.917	68.9	8.903	79.40	130.3	0.7
13	1125	0.0125	0.0079	12.711	70.5	8.957	89.22	131.1	0.7
14	1150	0.0111	0.0031	12.231	73.0	8.930	96.67	130.7	0.6
15	1175	0.0123	0.0039	12.827	71.3	9.141	98.17	133.7	0.8
16	1200	0.0171	0.0029	13.722	62.9	8.633	99.18	126.5	1.6
17	1225	0.0163	0.0004	13.843	64.8	8.971	99.73	131.3	2.5
18	1250	0.0172	0.0008	15.714	67.4	10.597	100.00	154.1	7.9
RO14 K-Feldspar; Otjohorong granite porphyry; 1.48 mg; J = 0.008405 ± 0.000025									
1	700	0.0671	0.0014	29.715	66.1	9.836	3.17	143.3	3.1
2	800	0.0187	0.0081	14.518	61.6	8.949	7.36	130.8	1.3
3	900	0.0120	0.0042	12.573	71.3	8.967	16.75	131.1	0.7
4	950	0.0059	0.0017	10.705	83.3	8.913	24.82	130.3	0.6
5	1000	0.0072	0.0012	11.123	80.6	8.961	34.55	131.0	0.6
6	1025	0.0092	0.0011	11.776	76.4	8.999	43.83	131.5	0.7
7	1050	0.0102	0.0011	12.048	74.6	8.989	52.29	131.4	0.7
8	1075	0.0097	0.0019	11.921	75.6	9.009	60.84	131.7	0.7
9	1100	0.0088	0.0017	11.725	77.3	9.064	71.35	132.5	0.6
10	1125	0.0077	0.0007	11.379	80.0	9.069	84.97	132.5	0.7
11	1150	0.0076	0.0001	11.342	79.7	9.039	92.46	132.1	0.7
12	1175	0.0095	0.0001	11.935	76.0	9.067	96.63	132.5	0.8
13	1200	0.0111	0.0001	12.438	73.2	9.110	98.48	133.1	1.0
14	1250	0.0118	0.0102	12.943	72.8	9.416	99.38	137.4	1.4
15	1300	0.0145	0.0193	13.367	67.7	9.045	100.00	132.2	1.9

132.3 ± 0.7 Ma. The Renne *et al.* (1996) ages are based on the Fish Canyon sanidine fluence monitor using an age of 27.84 Ma. This age is directly comparable to the GA-1550 age of 97.9 Ma used in the current study, (cf. Renne *et al.*, 1998).

When making comparisons with the U-Pb zircon data, it is necessary to take into account the uncertainties associated with age of the fluence monitor (~1%) and the error associated with the error in the K-Ar decay constants (~0.7%) (cf. Renne *et al.*, 1998). Inclusion of these errors, increases the uncertainties in the $^{40}\text{Ar}/^{39}\text{Ar}$ dates to approximately ±1.6 Ma. Despite these larger uncertainties, the U-Pb age for the Paresis porphyry is still older than the $^{40}\text{Ar}/^{39}\text{Ar}$ age for the same sample at the 95% confidence level. However, if the age of the GA-1550 fluence monitor is revised to 98.79 ± 0.96 Ma, as calculated by Renne *et al.* (1998), the plateau ages for the Paresis Complex and Otjohorong porphyry increase to 131.8 ± 1.6 Ma and 132.8 ± 1.5 Ma, respectively. The latter results are within error of the U-Pb ages and the mean age for the Paresis Complex, based on both techniques, becomes 133.0 ± 1.2 Ma.

The Erongo Volcanic Complex

The Erongo Volcanic Complex (EVC) is a well preserved caldera structure surrounded by a granitic ring dyke and a mafic cone sheet (Fig. 4). The EVC is the

largest of the Damaran alkaline ring complexes with the caldera structure having a diameter of approximately 30 km, but if the gabbro cone sheet is included the diameter is more than 50 km. The geology of the Complex was described in detail by Blümel *et al.* (1979) and Pirajno (1990).

The EVC was emplaced through a basement of fault-bounded blocks of granitic rocks and metasedimentary rocks of Damaran age and on which immature Karoo clastic sedimentary rocks had accumulated in small basins, perhaps just prior to the commencement of volcanic activity. The EVC magmatism is characterised by two phases: 1) an early mafic phase, which consists of a succession of tholeiitic lavas, dykes and the above-mentioned gabbroic cone sheet; and 2) a later felsic phase, which consists of pyroclastic flows of dacitic to rhyolitic composition. A first estimate of the age of the EVC was a whole-rock Rb-Sr isochron from a sample of ring dyke granite (Erongo Granite), which yielded an age of 143.6 ± 2 Ma (Late Jurassic; McNeill, 1989). Our new U-Pb SHRIMP dating of zircons from the Ombu Ash Flow Tuff (OAF; see below) yielded a mean age of 135.3 ± 3.2 (1σ) (Fig. 2B).

The early mafic phase is the result of voluminous effusions of tholeiitic lavas, which formed a platform, whose areal extent may have been much greater than the present-day distribution. This is suggested by the presence of the Krantzberg lava outlier to the northeast,

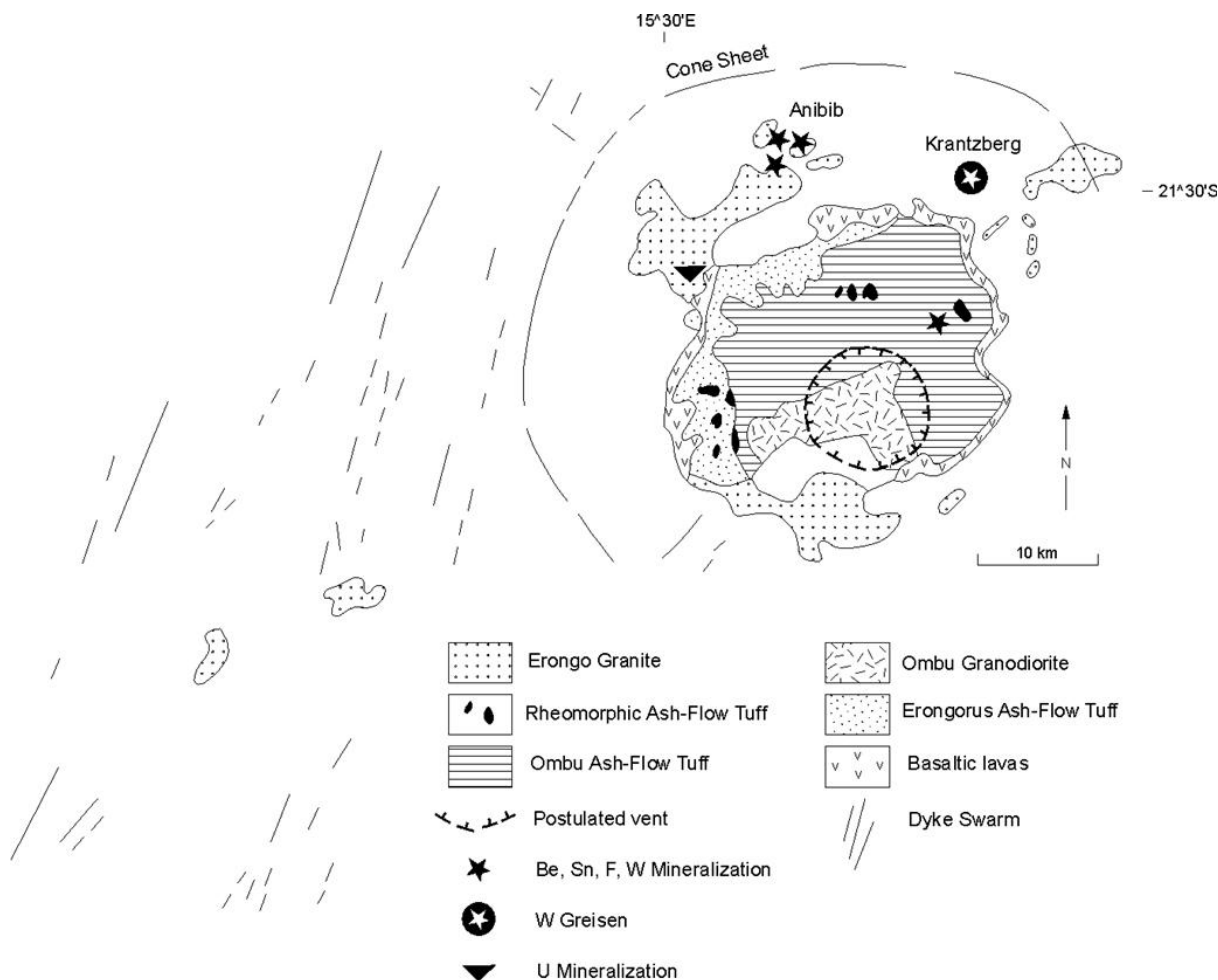


Figure 4: Simplified geology of the Erongo Volcanic Complex and distribution of mineral deposits and occurrences. After Pirajno (1990; 1994). Also shown is a dyke swarm on the west side of the Complex; the cone sheet and dykes may have been the feeders of the tholeiite lavas that form the base of the Complex.

which is spatially associated with greisen-style mineralisation (see below). The thickness of the lava succession is between 200 and 300 m and on this lava pile, the subsequent felsic volcanic products accumulated. The feeders of these tholeiitic lavas may have been the gabbroic cone sheet and a number of radial dykes that outcrop to the south and the northeast of the caldera. In addition, a swarm of NNE-trending mafic dykes cut through the Damaran basement to the west of the EVC (Fig. 4). In the upper parts of the lava pile, the composition becomes trachytic and the lavas become intercalated with the earliest pyroclastic units, suggesting that these uppermost trachytic lava flows heralded a change in the composition of the magma towards a more felsic type.

Rocks of the felsic phase are dominated by voluminous pyroclastic deposits which, based on stratigraphic, petrographic and geochemical evidence, can be subdivided into three distinct sequences (Pirajno, 1990). From oldest to youngest, they are: Erongorus ash-flow tuff (EAFT), Ombu ash-flow tuff (OAFT) and rheomorphic rhyolitic rocks (RHEOR). The EAFT represents the first explosive event of the Erongo Complex, char-

acterised by having only juvenile material, no lithics and abundant vesicles and lithophysae. The thickness of the EAFT sequence is estimated at between 200 and 370 m, and the composition ranges from andesitic in the lower levels to rhyodacitic at the top. The OAFT is volumetrically the major rock type of the EVC, reaching a thickness of at least 500 m. In the east, northeast and southeast the OAFT rests on the basal tholeiitic lavas, whereas in the central and western areas it overlies the EAFT. OAFT rocks are characterised by having abundant crystal and lithic fragments and have compositions ranging from dacitic to rhyodacitic. RHEOR rocks form isolated outliers that generally overlie EAFT and OAFT units. Field relationships, however, indicate that the RHEOR were emplaced on a rugged topography, most probably the outer slopes of the volcanic edifice, which were cut by deep valleys. RHEOR rocks have a rhyolitic composition and are characterised by fine laminations, interpreted as flow banding. Tourmaline is present as fine overgrowths and along microfractures. The presence of tourmaline in the RHEOR rocks and their chemistry suggest that they may be genetically related to the tourmaline-rich Erongo Granite.

Subvolcanic rocks of the EVC include the Ombu Granodiorite and the Erongo Granite. The Ombu Granodiorite occurs in the south-central EVC where it occupies a topographic depression. It is a coarse to fine-grained monzogranite to granodiorite containing numerous xenoliths of the same type as the lithic fragments in the OAFT. On the basis of field relationships, geochemical and petrographic data, the Ombu Granodiorite is the subvolcanic equivalent of the OAFT rocks (Pirajno, 1990). The topographic depression that the granodiorite occupies is interpreted as the outline of the vent through which the felsic phase of the EVC erupted. The Ombu Granodiorite locally exhibits hydrothermal alteration, of which two trends can be recognised: potassic (K-feldspar + biotite) and phyllic-propylitic (sericite + chlorite + tourmaline). The Erongo Granite forms plutons distributed between the granite ring dyke and the caldera structure. The plutons are interpreted to represent the remnants of a ring dyke. The main rock type is a coarse-grained biotite granite, containing abundant topaz and tourmaline and minor apatite and fluorite. The Erongo Granite has an A/CNK ratio (defined as $Al_2O_3/CaO + Na_2O + K_2O$ mol. Wt.%) of between 1.08 and 1.17 and is therefore peraluminous (McNeill, 1989).

A prominent feature of the Erongo Granite is the presence of disseminated quartz-tourmaline veins, stringers and nests up to 30 cm in diameter, all of which tend to increase in abundance and to coalesce towards the upper parts of the plutons. In addition to tourmaline and quartz, the nests also contain topaz, fluorite, apatite and cassiterite. Quartz-tourmaline breccias and dyke-like bodies cut through and locally replace rocks of the Damara Sequence all around the EVC.

To the northeast of the EVC, lamprophyre dykes crop out and converge towards a cluster of small (up to 100 m in diameter), undersaturated mafic plugs. This area is coincident with a positive gravity anomaly.

Mineralisation

The EVC contains deposits and occurrences of W–F–Sn, W, Be, Sn, F, and U, all of which are spatially and genetically related to the Erongo Granite. The distribution of the principal deposits is shown in Figure 4. The mineralisation associated with the EVC was described by Pirajno and Schögl (1987) and Pirajno (1990). A brief review of this mineralisation, summarised from the above authors, is given below.

Be and Sn mineralisation, hosted by a quartz-albite rock containing numerous tourmaline veins and nests, is present to the north of the EVC (Etemba farm). This mineralisation is associated with quartz-muscovite (greisen) alteration containing minor cassiterite disseminations. Drusy pegmatitic pods with crystals of beryl and tourmaline are also present. The quartz-albite rock is probably an alteration zone in a high level (cupola) facies of the Erongo Granite. Rocks around the

mineralised locality are brecciated and are cut by veins of tourmaline, attesting to hydraulic fracturing induced by B-rich fluids.

About 1 km west of the Be–Sn occurrence, a north-west-trending, 50 m-long mineralised fracture in Damaran granite contains a core of quartz-sericite with symmetrical bands of quartz-tourmaline rock. Wolframite is present within the quartz-sericite material.

To northwest of the EVC (Anibib farm), along the contact zone between the Erongo Granite and Damaran granitic rocks, there is a zone of intense brecciation and tourmalinisation associated with albitisation. This area contains Sn (cassiterite), W (unknown mineral phase) and fluorite mineralisation.

Low-grade U mineralisation is present in the Erongo Granite, particularly in the northwest and southwestern areas. Secondary U minerals are associated with jointing in areas of primary U enrichment (Potgieter, 1987). It is probable that this mineralisation is due to oxidising meteoric waters that have leached U from the fresh Erongo Granite in areas of high permeability due to close-spaced jointing.

The Krantzberg W–F–Sn deposit

The old Krantzberg mine was a major tungsten producer in Namibia. Mining operations ceased in 1979 and subsequent exploration did not define additional economically feasible grades and tonnages. Mineralisation at Krantzberg consists of W (ferberite), F (fluorite), minor Sn (cassiterite), Mo, Fe, and Cu sulphides. This mineralisation is hosted in replacement-type greisen rocks and quartz-tourmaline breccias.

The style of the Krantzberg deposit is shown in Figure 5. The ‘Krantzberg’ is a prominent hill of rocks of the Damara Sequence that was protected from erosion by an overlying cap of clastic sedimentary rocks of Karoo age, and an outlier of EVC basaltic rocks (Figs. 4 and 5). There are three main zones of alteration–miner-

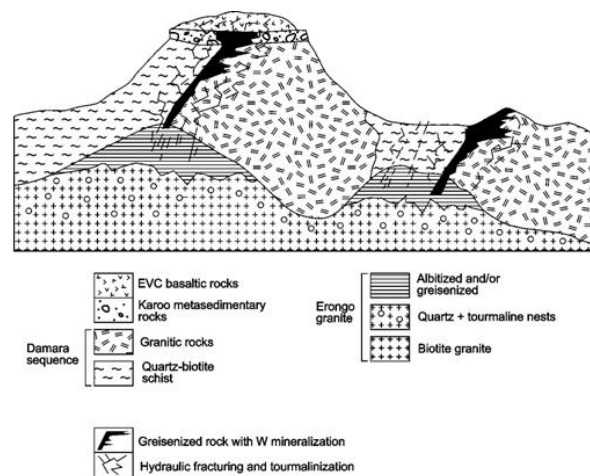


Figure 5: Schematic cross-section of the Krantzberg greisen-style W deposits. After Pirajno and Schögl (1987).

alisation, all formed by the pervasive greisenisation of Damaran granites. The Krantzberg greisen alteration is interpreted to be the result of acidic fluids that emanated from the subsurface apical portions of fractionated Erongo Granite cupolas. The mineralising fluids were also B- and F-rich and induced extensive selective replacement of pre-existing granite lithologies by quartz, sericite, topaz and tourmaline. Late-stage veins contain ore minerals such as ferberite, scheelite and minor sulphides.

Breccia pipes on the southeastern slopes of the Krantzberg contain fragments of volcanic rocks cemented by quartz and tourmaline. Cassiterite occurs as fine disseminations or as patches along the periphery of the breccia bodies. These breccias are interpreted as a type of hydraulic fracturing due to streaming of B-rich fluids.

Volcanic history

A model showing a suggested sequence of events that formed the EVC is schematically depicted in Figure 6. The volcanic history of the EVC probably began soon after the inception of block faulting and the deposition of immature clastic sediments in an area of crustal instability, perhaps due to a combination of tectonic movements related to the pressure exerted by uprising magma (Fig. 6A). Outpouring of tholeiitic lavas took place from several different feeders (Fig. 6B). The absolute age of the lavas is not known. The extrusion of the basaltic lavas was followed by a phase of felsic volcanic activity, characterised by voluminous eruptions of pyroclastic material (Fig. 6C and D). The three pyroclastic sequences (EAFT, OAFT, RHEOR) represent distinct events, which rapidly succeeded one another. The absence of intervening or intercalated sedimentary rocks attests to high eruption rates. The oldest is the EAFT sequence, which began with a transitional episode characterised by alternate eruptions of mafic-intermediate lavas and thin sheets of ash-flow tuffs. With time, the nature of EAFT volcanism became progressively more explosive and more acidic, with no more lava flows (Fig. 6C). The general character of the EAFT rocks indicates that they were volatile-rich and emplaced at high temperature. The EAFT volcanism can be envisaged as one of fairly dense pyroclastic material with short eruption columns and a small gas-thrust component, erupted in a fountain-like fashion. The movement of the pyroclastic flows was towards the west and the north, from a vent possibly situated in the Ombu area. A resurgence of mafic magmatism occurred towards the end of the EAFT event and the beginning of the OAFT event. This resulted in the emplacement of gabbroic sills and lavas at the contact between the two pyroclastic series (Fig. 6D). The fact that these mafic rocks are only found in the northwestern areas (Omandumba), confirms that the northern side of the EVC was an area of continuing tectonic instability.

The Ombu event (OAFT sequence) is represented by a series of ignimbrite eruptions (Fig. 6D). Outliers of OAFT units in the vicinity of Krantzberg, in the north-east, indicate that OAFT units must have had a greater areal extent than that inferred by the present-day exposures within the confines of the caldera-like structure. In the southern part of the EVC, the OAFT surrounds and grades into the Ombu granodiorite. The Ombu Granodiorite occupies a vent area that now forms the Ombu plains. Central eruptions of OAFT rocks may have come from a shallow magma chamber. The eruption column was probably sub-Plinian in character with a greater gas-thrust component than the EAFT columns. Nevertheless, the absence of air-fall pyroclastics suggest that the OAFT columns were only high enough to cause gravitational collapse resulting in pyroclastic flows. The absence of recognisable base surge deposits suggests that there was little or no interaction with groundwater, and that the energy was entirely provided by the volatile content of the magma. There must have been several individual flows to account for the present-day thickness of at least 500 m. The pyroclastic flows accumulated rapidly and welded onto one another form-

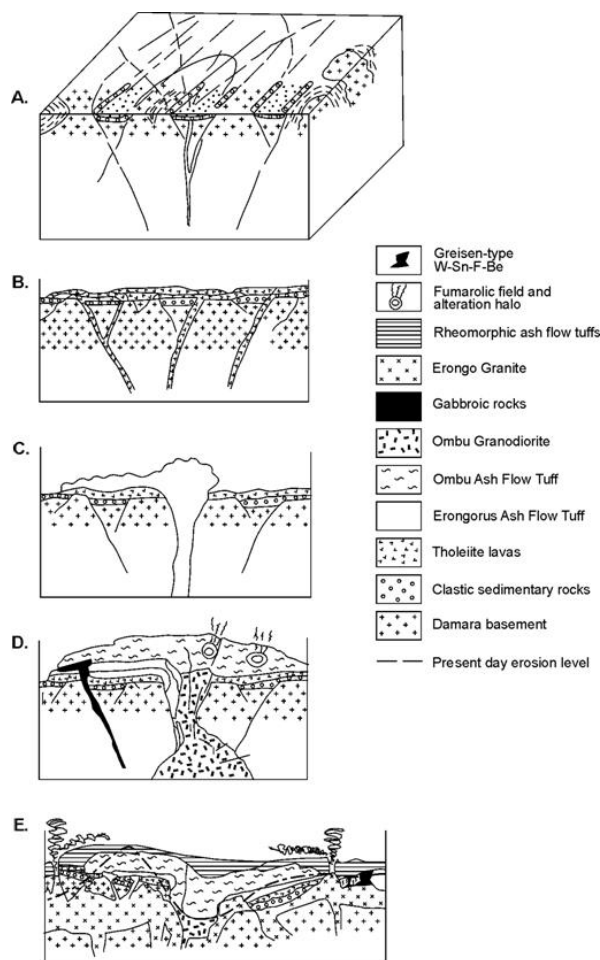


Figure 6: Interpreted volcanic history of the Erongo Volcanic Complex. After Pirajno (1990). Figures not to scale. See text for details.

ing thick cooling units. Degassing of the cooling units resulted in fumarolic activity with alteration and localised mineralisation (mainly fluorite disseminations).

The emplacement of the Erongo Granite took place sometime after the last OAFTE eruption. It is postulated that below the present surface the Erongo Granite forms a continuous mass above and around subsided blocks of volcanic and basement rocks (Fig. 6E). The Erongo Granite is important from the metallogenic viewpoint because it acted both as heat engine and as source for hydrothermal fluids which were H₂O-poor but rich in alkalis, B and F. Widespread metasomatism occurred with local greisen-type mineralisation containing W, Sn, F and Be, hosted in the roof zones of the granite and in the surrounding country rocks.

The rheomorphic rhyolitic rocks (RHEOR), representing the third volcanic event, may be the effusive equivalent of the Erongo Granite. If this interpretation is correct, then the eruption of the RHEOR units must have occurred from a ring fracture outside the central volcanic edifice. This ring fracture, at the present level of exposure is occupied by the Erongo Granite (Fig. 6E). Collapse of the volcanic edifice at about this time led to the formation of the caldera-like structure and the tilting of the rock units towards the centre of the complex. Estimates, based on the highest and lowest points of the base of the RHEOR, suggest that a collapse of at least 500 m may have occurred. Various lines of evidence also suggest that the RHEOR are high-temperature ignimbrites or ash flow tuffs (see Pirajno, 1990). Similar high-temperature ignimbrites are present in the Etendeka Formation (rheoignimbrite flows; Milner, 1988; Milner *et al.*, 1992).

The final stage in the EVC geological history was the emplacement of alkaline mafic dykes and the undersaturated mafic plugs that intrude the pyroclastic sequences in the northeastern areas. It is possible that these may represent a resurgence of alkaline mafic magmatism due to re-activation of deep-seated fractures. However, the relevance of this late magmatism, in terms of petrogenesis, to the evolution of the EVC is not clear.

The Paresis Igneous Complex

The Paresis Igneous Complex (PIC) consists of alkaline volcanic and sub-volcanic rocks which were emplaced at approximately 136-137 Ma (Manton and Siedner, 1967; Milner *et al.*, 1995) through a basement of metasedimentary rocks of the Damara Sequence. Results of U-Pb SHRIMP analysis of zircons from quartz-feldspar porphyry rocks yielded an average of 134.3±1.7 Ma (1σ) (Fig.2A).

The PIC was studied in detail by Siedner (1965a and b). Later investigations, focussed mainly in the southern and eastern parts of the complex (Roesener, 1989; Pirajno *et al.*, 1990). A simplified geological map of the PIC is shown in Figure 7. The PIC has a diameter of about 17 km and is surrounded by three ring faults. The com-

plex consists of lavas and pyroclastic flows, dominantly of rhyolitic composition, which include feldspar-porphphyry, quartz-feldspar porphyry and comendites. Plutonic rocks include microgranite, syenite and bostonite, generally associated with the ring faults. Geochemical analyses of syenitic rocks indicate that they are strongly peralkaline, having A/CNK ratios of between 0.74 and 0.82 (McNeill, 1989).

Under the term of “feldspar porphyry”, Siedner (1965a) included massive lava flows as well as welded pyroclastic flows. The feldspar porphyry (also called feldspar rhyolite) is characterised by alkali feldspar phenocrysts, which have a plagioclase core mantled by alkali feldspar in a brown devitrified matrix. Devitrification spherulites, some up to 1 m in diameter, commonly form distinct horizons within a given flow unit. Some spherulites have been interpreted as accretionary lapilli, suggesting steam-driven pyroclastic columns of phreato-magmatic eruptions (Roesener, 1989). The quartz-feldspar porphyry is generally massive and is characterised by quartz, plagioclase and K-feldspar phenocrysts in a variably coloured aphanitic groundmass. The comendite is volumetrically the most abundant rock type, locally displaying pyroclastic textures typical of strongly welded ash flow tuffs. It is charac-

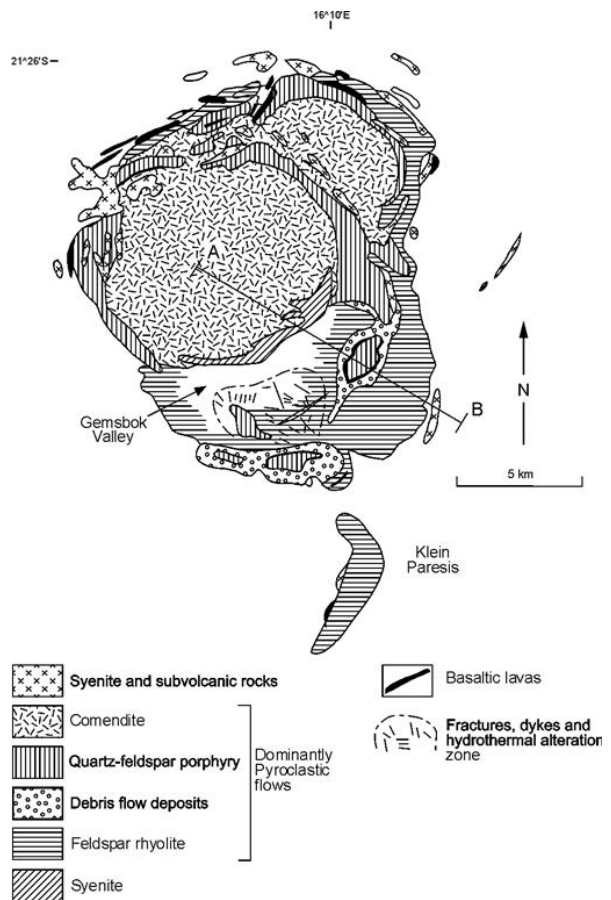


Figure 7: Simplified geological map of the Paresis Igneous Complex. After Siedner (1965a and Pirajno *et al.*, 1990). Cross-section along A-B is shown in Figure 8.

terised by the presence of riebeckite phenocrysts set in a granular groundmass composed of quartz and K-feldspar. In places, hornblende and aegirine are also present and are set in a fine groundmass of quartz and feldspar. On the basis of the presence of eutaxitic textures and fiamme, this rock is interpreted as a pyroclastic flow. The syenite is a medium- to coarse-grained rock containing about 75 % by volume alkali feldspar with minor quartz, clinopyroxene, fayalitic olivine and more rarely hornblende. The syenite is present only in major fractures suggesting that it was emplaced late in the volcanic history of the complex, perhaps during the caldera collapse stages. Bostonite forms small plugs and narrow dykes in the northern part of PIC. Microgranite ring dykes are present along the outermost ring fracture, which forms an almost perfect circle some 17 km in diameter. A composite stock composed of tinguaita, phonolite and foyaite is present in the northwestern part of the PIC. Basaltic lavas and gabbros are present as minor components.

The southeastern portion of PIC is characterised by feldspar- and quartz-feldspar (plagioclase and K-feldspar) porphyry rocks intercalated with debris-flow deposits (agglomerate of Siedner 1965a) and basaltic lavas. This area was studied in detail by Roesener (1989) who interpreted most of the porphyry rocks as welded ignimbrites. The feldspar porphyries, occupying topographically low areas (Gemsbok Valley), are cut by the northeast-trending Gemsbok Fault and are overlain by debris flow deposits with intercalated basaltic lavas. The debris flows are in turn overlain by quartz-feldspar porphyry rocks. The debris-flow units are mixtures of massive to well bedded fine and very coarse material, with thicknesses of about 100 m. They contain porphyry clasts from a few cm to 2 m in diameter set in an unsorted coarse, unwelded matrix of sand-size lapilli. Feldspar and quartz phenocrysts in the matrix are angular and fractured and range in size from 0.1 to 3 mm in size. The tops and more distal portions of debris-flow units exhibit bedding, whereas the central

zones contain large, rotated porphyry blocks up to tens of metres across. The debris-flow units are interpreted to have formed as an avalanche resulting from an initial rotational slump that slid down a slope, similar to those that occurred during the Mt St Helens eruption (Janda *et al.*, 1981; Roesener, 1989).

The feldspar porphyry that crops out in the Gemsbok Valley is typically fractured and hydrothermally altered. This alteration is manifest by pervasive argillisation, Fe and Mn oxides, local silicification and quartz-sericite-pyrite. An idealised section through the valley is shown in Figure 8.

Volcanic history

The volcanic history (Fig. 9) of the PIC commenced with the central eruption of lavas and pyroclastic flows (feldspar porphyry) (Fig. 9A). In the northern part of the PIC, basaltic lavas are intercalated with these rocks but it is possible that they were extruded from a different source. This event resulted in the construction of the main volcanic edifice (Fig. 9B).

In the next phase, deposition of pyroclastic units, interpreted as debris-flows, took place (Pirajno *et al.*, 1990) (Fig. 9C). These debris-flows were probably derived from the collapse of the volcanic edifice, possibly due to a burst of explosive activity on the flank of the crater, resulting from mixing of magma with groundwaters. The eruption of extensive ash-flows tuffs (quartz-feldspar porphyry) was triggered by the collapse of portions of the volcanic edifice (Fig. 9C and D). The last paroxysmic episode was the eruption of the comendites (Fig. 9E). Caldera collapse followed the eruption of the

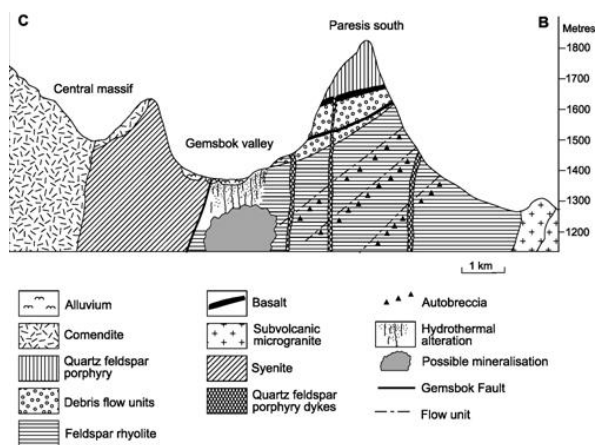


Figure 8: Cross-section through Gemsbok Valley (after Roesener, 1989) showing the exposed area of hydrothermal alteration and inferred buried mineralised zone.

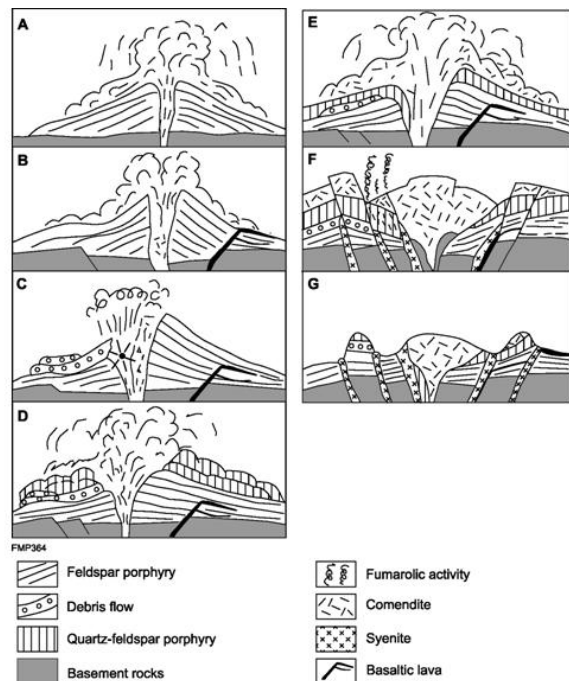


Figure 9: Interpreted volcanic history of the Paresis Igneous Complex. After Pirajno *et al.* (1990). See text for details.

comendites, which was more or less coeval with the intrusion of syenite and microgranitic dyke-like bodies along ring fractures (Fig. 9F). Fumarolic activity may have occurred at this time and was mainly concentrated on the southern flank of the newly formed caldera (Fig. 9F). No intercalated sedimentary material (e.g. paleosols) was observed in the pyroclastic sequences studied, the same as for the Erongo Volcanic Complex. This feature suggests that the Paresis volcanism was of short duration. Figure 9G schematically illustrates the present-day configuration of the PIC.

Evidence of hydrothermal activity can be seen in the southern portions of the PIC (Gemsbok Valley). This is a deeply eroded area that is traversed by the north-east-trending Gemsbok Fault. In this area, the rocks have been silicified and/or altered to an assemblage of quartz + sericite + pyrite. Sulphur isotopic analysis of this pyrite gave values of + 1.2 $\delta^{34}\text{S}$ per mil suggesting a magmatic source for the sulphur (Pirajno *et al.*, 1992). The Gemsbok Valley area is also characterised by intense fracturing and dyke emplacement. The fractures enhanced the permeability of the rocks permitting the circulation of hydrothermal fluids. No quartz veins are present in the area. This indicates a low level of erosion or lack of a sustained convective hydrothermal cell which could have dissolved, carried and deposited silica in the fractures. Alternatively, the fluids were circulating in highly porous material which inhibited the formation of fractures. Hydrothermal activity and associated alteration in the Gemsbok valley suggest potential for porphyry epithermal-style mineralisation.

Discussion and Conclusions

Continental flood basalts and related rocks in the Paraná basin of Brazil and adjoining areas in Paraguay and Uruguay are chronologically (~127-137Ma) and geologically continuous with the Etendeka province in Namibia (Peate, 1997). The Paraná-Etendeka magmatism is bimodal (rhyolitic-basaltic) and is related in space and time to the upwelling of the Tristan da Cunha mantle plume and continental rifting. Earlier alkaline magmatism (~135-144 Ma) took place along the continental extension of transform faults inland and away from the rift that was to develop into the South Atlantic Ocean (Peate, 1997). We suggest that hot plume material could have penetrated laterally along weak zones beneath the Neoproterozoic Damara orogenic belt. The Erongo Volcanic Complex and the Paresis Igneous Complex are part of this early alkaline magmatic event. SHRIMP U-Pb results on zircons from the OAFT and quartz-feldspar porphyry, respectively from the EVC and PIC, indicate eruption ages in the range of 135-134 Ma. Step-heating $^{40}\text{Ar}/^{39}\text{Ar}$ on K-feldspars from the Paresis Complex revealed a younger plateau age of about 132 Ma. These ages confirm the chronological correlation with the Paraná-Etendeka magmatic event.

Based on field evidence, we suggest that this type of

plume-related intracontinental volcanism is short-lived and predominantly explosive. The character of this explosive volcanism is linked to the composition of the magma, volatile content and the possible interaction of the magma with surface water and groundwater. In the case of the EVC a dry magma did not interact with surface water and groundwater to any great extent. A deep-seated granitic melt was rapidly intruded along a ring fracture late in the history of the complex. This melt vented at the surface as high-temperature ash-flow tuffs or rheoignimbrites. Below the surface, crystallisation of this water-poor but F- and B-rich magma resulted in intense autometasomatism and greisenisation of the surrounding rocks. This metasomatism produced a greisen-style W, Sn and F mineralisation.

The magma of the Paresis complex, although also of a dry nature, shows evidence of having interacted with both groundwater and surface water. This evidence is provided by the water-worked debris-flow deposits on the southern flank of the complex and the nature of the extensive zone of hydrothermal alteration in the Gemsbok Valley. This alteration, mainly quartz-sericite-pyrite and silicification, is similar to that encountered in magmatic, arc-related epithermal and porphyry systems. Epithermal and/or porphyry-type deposits have not been reported from intracontinental anorogenic complexes. However, the rich Au-Te deposits at Cripple Creek, Colorado (USA) are typically associated with alkaline complexes, emplaced at approximately 30 Ma, and related to extensional tectonics (Kelley, 1998; Saunders 1998; Thompson 1998). It is considered possible that the Paresis complex may host this type of mineralisation. In addition, consideration should also be given to the possibility of a porphyry system at shallow depths. Examples of continental flood basalt and rift-related porphyry systems are little publicised. One of these examples is the Bolgokhtokhsy Cu-Mo porphyry deposit in Siberia, associated with the Permo-Triassic Siberian Traps (Strunin *et al.*, 1992). Another example is provided by the Mo-dominated porphyry systems of the Oslo rift, which are also related to ring-type volcano-plutonic structures of rhyolitic, syenitic and basaltic composition with quartz-feldspar porphyries and characterised by voluminous ash flow tuffs (Schonwandt and Petersen, 1983).

Both the EVC and the PIC lack fluid inclusion, stable isotope and trace element studies such as those carried out by Ewart *et al.* (1998a and b) for the Messum Complex. These studies are necessary and would be instrumental in providing important data to improve our understanding of these fascinating igneous systems, their possible link with mantle activity and their mineral resource potential.

Acknowledgements

FP publishes with the permission of the Director of the Geological Survey of Western Australia. The au-

thors thank two referees, Drs. A. Le Roex and J. B. Loewensten, for their constructive comments.

References

- Blümel, W.D., Emmerman, R. and Huser, K. 1979. Der Erongo. Geowissenschaftliche Beschreibung und Deutung eines südwestafrikanischen Vulkankomplexes. *Scient. Res. SWA Ser., S. W. Af. scient. Soc.*, **16**, 140 pp.
- Compston W., Williams I.S., Kirschvink J.L., Zhang Z. and Ma, G. 1992. Zircon U-Pb ages for the Early Cambrian time-scale. *J. geol. Soc., London*, **149**, 171-184.
- Cumming, G.L. and Richards, J.R. 1975. Ore lead isotope ratios in a continuously changing earth. *Earth Planet. Sci. Lett.*, **28**, 155-171.
- Diehl, M. 1990. Geology, mineralogy, geochemistry and hydrothermal alteration of the Brandberg Alkaline Complex, Namibia. *Mem. geol. Surv. Namibia*, **10**, 55 pp.
- Ewart, A., Milner, S.C., Armstrong, R.A. and Duncan, A.R. 1998a. Etendeka volcanism of the Goboboseb Mountains and Messum Igneous Complex, Namibia. Part I: geochemical evidence of Early Cretaceous Tristan Plume melts and the role of crustal contamination in the Parana-Etendeka CFB. *J. Petrol.*, **39**, 191-225.
- Ewart, A., Milner, S.C., Armstrong, R.A. and Duncan, A.R. 1998b. Etendeka volcanism of the Goboboseb Mountains and Messum Igneous Complex, Namibia. Part II: voluminous quartz latite volcanism of the Awahab magma system. *J. Petrol.*, **39**, 227-253.
- Erlank, A.J., Marsh, J.S., Duncan, A.R., Miller, R.McG., Hawkesworth, C.J., Betton, P.J. and Rex, D.C. 1984. Geochemistry and petrogenesis of the Etendeka volcanic rocks from SWA/Namibia. *Spec. Publ. geol. Soc. S. Afr.*, **13**, 195-245.
- Janda, R.J., Scott, K.M., Nolan, K.M. and Martinson, H.A. 1981. Lahar movements, effects and deposits. *U. S. geol. Surv. Prof. Pap.*, 1250.
- Kelley, K.D. 1998. Geochemical and geochronological constraints on the genesis of Au-Te deposits at Cripple Creek, Colorado, USA. *Geol. Soc. Am., 1998 Annual Meeting, Abstracts with Programs*, A-204.
- Ludwig, K.R. 1999. Isoplot/Ex version 2.00: A Geochronological Toolkit for Microsoft Excel. *Berkeley Geochron. Center, Spec. Publ.*, **1a**, 46 pp.
- MacDougall, I. and Harrison, T.M. 1999. *Geochronology and thermochronology by the ⁴⁰Ar/³⁹Ar method*. Second Edition. Oxford Univ. Press, New York.
- MacDougall, I. and Roksandic, Z. 1974. Total fusion ⁴⁰Ar/³⁹Ar ages, HIFAR reactor. *J. geol. Soc. Austr.*, **21**, 81-89.
- Manton, W.I. and Siedner, G. 1967. Age of the Paresis Complex, South-West Africa. *Nature*, **216**, 1107-1198.
- McNeill, G.W. 1989. *A geochemical study of three Namibian igneous complexes*. Unpubl. BSc. (Hons) thesis, Univ. St. Andrews, 57 pp.
- Miller, R.McG. 1980. Geology of a portion of central Damaraland, South West Africa/Namibia. *Mem. geol. Surv. S. Afr., S.W. Afr. Ser.*, **6**, 78 pp.
- Milner, S.C. 1988. *The geology and geochemistry of the Etendeka Formation quartz latites, Namibia*. Unpubl. PhD thesis, Univ. Cape Town, 244 pp.
- Milner, S.C., Duncan A.R. and Ewart, A. 1992. Quartz latite rheoignimbrite flows of the Etendeka Formation, northwestern Namibia. *Bull. Volcanol.*, **54**, 200-219.
- Milner, S.C., Le Roex, A.P. and O'Connor, J.M. 1995. Age of Mesozoic igneous rocks in northwestern Namibia, and their relationship to continental breakup. *J. geol. Soc., London*, **152**, 97-104.
- Paces, J.B. and Miller, J.D. 1989. Precise U-Pb ages of Duluth Complex and related mafic intrusions, Northeastern Minnesota: Geochronological insights to physical, petrogenic, paleomagnetic and tectonomagmatic processes associated with the 1.1 Ga midcontinent rift system. *J. geophys. Res.*, **98B**, 13997-14013.
- Peate, D.W. 1997. The Paraná-Etendeka Province. In: J.J. Mahoney, and M.F. Coffin (eds), *Large Igneous Provinces – continental, oceanic and planetary flood volcanism*. Am. Geophys. Union Monogr., **100**, 217-246.
- Pirajno, F. 1990. The geology, geochemistry and mineralisation of the Erongo Volcanic Complex, Namibia. *S. Afr. J. Geol.*, **93**, 485-504.
- Pirajno, F. 1994. Mineral resources of anorogenic alkaline complexes in Namibia: a review. *Aust. J. Earth Sci.*, **41**, 157-168.
- Pirajno, F. and Schlögl, H.U. 1987. The alteration-mineralization of the Krantzberg tungsten deposit, South West Africa/Namibia. *S. Afr. J. Geol.*, **90**, 239-255.
- Pirajno, F., Roesener, H. and Petzel, V.W.F. 1990. The volcanic history of the Paresis Igneous Complex. *Geol. Soc. S. Afr., Geocongress '90, Extended Abstracts*, 447-450.
- Pirajno, F., Kinnaird, J.A., Fallick, A.E., Boyce, A.J. and Petzel, V.W.F. 1992. A preliminary regional sulphur isotope study of selected samples from mineralised deposits of the Damara Orogen, Namibia. *Commun. geol. Surv. Namibia*, **8**, 81-97.
- Potgieter, J. E. 1987. *Anorogenic alkaline ring-type complexes of the Damaraland province, Namibia, and their economic potential*. Unpubl. MSc. thesis, Rhodes Univ., Grahamstown, 150 pp.
- Prins, P. 1981. The geochemical evolution of the alkaline and carbonatite complexes of the Damaraland Igneous Province, South West Africa. *Ann. Univ. Stellenbosch, Ser. A1* (**3**), 145-278.
- Renne, P.R., Glen, J.M., Milner, S.C. and Duncan, A.R. 1996. Age of the Etendeka flood volcanism and associated intrusions in southwestern Africa. *Geology*, **24**, 659-662.

- Renne, P.R., Swisher, C.S., Deino, A.L., Karner, D.B., Owens, T.L. and DePaolo, D.J. 1998. *Chem. Geol.*, **145**, 117-152.
- Roesener, H. 1989. *The pyroclastic sequences of the Paresis Igneous Complex, Namibia*. Unpubl. BSc. (Hons) thesis, Rhodes Univ., Grahamstown, 43 pp.
- Saunders, J.A. 1998. Tectonic setting, petrology and mineralogy of "alkalic" gold telluride deposits of the Colorado Mineral Belt. *Geol. Soc. Am., 1998 Annual Meeting, Abstracts with Programs*, A-204.
- Schonwandt, H.K. and Petersen J.S. 1983. Continental rifting and porphyry molybdenum occurrences in the Oslo region, Norway. *Tectonophysics*, **94**, 609-631.
- Siedner, G. 1965a. Structure and evolution of the Paresis Igneous Complex, South West Africa. *Trans. geol. Soc. S. Afr.*, **168**, 177-202.
- Siedner, G. 1965b. Geochemical features of a strongly differentiated alkali igneous suite. *Geochim. Cosmochim. Acta*, **29**, 113-137.
- Smithies, R.H. and Marsh, J.M. 1998. The Marinkas Quelle Carbonatite Complex, southern Namibia; carbonatite magmatism with an uncontaminated depleted mantle signature in a continental setting. *Chem. Geol.*, **148**, 201-212.
- Steiger, R.H. and Jaeger, E. 1977. Subcommission on geochronology: convention on the use of decay constants in geo- and cosmochronology. *Earth Planet. Sci. Lett.*, **36**, 359-362.
- Strunin, B.M., Distler, V.V. and Mkrtychyan, A.K. 1992. Porphyry copper ore formation, 175-190. In: Duzhikov, O.A., Distler, V.V., Strunin, B.M., Mkrtychyan, A.K., Sherman, M.L., Sluzhenikin, S.S. and Lurye, A.M. (eds), *Geology and metallurgy of sulfide deposits, Noril'sk region, U.S.S.R.* Spec. Publ. Soc. Econ. Geol., **1**, 242 pp.
- Tera, F. and Wasserburg, G.J. 1972. U-Th-Pb systematics in three Apollo 14 basalts and the problem of initial Pb in lunar rocks. *Earth Planet. Sci. Lett.*, **14**, 281-304.
- Tetley, N., MacDougall, I. and Heydegger, H.R. 1980. Thermal neutron interferences in the $^{40}\text{Ar}/^{39}\text{Ar}$ dating technique. *J. geophys. Res.*, **85**, 7201-7205.
- Thompson, T.B. 1998. Cripple Creek – a world class gold-bearing diatreme – alkalic intrusive complex, Colorado, USA. *Geol. Soc. Am., 1998 Annual Meeting, Abstracts with Programs*, A-204.
- Watkins, R.T., MacDougall, I. and Le Roex, A.P. 1994. K-Ar ages of the Brandberg and Okenyenya igneous complexes, north-western Namibia. *Geol. Rundsch.*, **83**, 348-356.
- Williams, I.S. and Claesson, S. 1987. Isotopic evidence for the Precambrian provenance and Caledonian metamorphism of high-grade paragneisses from the Seve Nappes, Scandinavian Caledonides. II. Ion microprobe zircon U-Th-Pb. *Contrib. Mineral. Petrol.*, **97**, 205-217.

Appendix 1

Analytical details

U-Pb Methods

The zircons were separated at the Research School of Earth Sciences (RSES), Australian National University, using standard heavy liquid and magnetic techniques. Handpicked zircons from each sample were mounted in epoxy together with the zircon standard AS3 (Duluth Complex gabbroic anorthosite; Paces and Miller, 1989) and the RSES standard SL13. The grains were sectioned approximately in half, polished and photographed. Selection of spots for analysis on the SHRIMP were made with the aid of normal transmitted and reflected light microphotographs as well SEM cathodoluminescence (CL) images.

The U-Th-Pb analyses were performed on the SHRIMP I at the RSES, and the data reduced in a manner similar to that described by Compston *et al.* (1992) and Williams and Claesson (1987). U/Pb in the unknowns were normalised to a $^{206}\text{Pb}/^{238}\text{U}$ value of 0.1859 (equivalent to an age of 1099.1 Ma) for AS3 using an empirical quadratic calibration. The U and Th concentrations were determined relative to those measured in the SL13 standard. U/Pb ages were calculated from the radiogenic $^{206}\text{Pb}/^{238}\text{U}$ ratios, using the decay constants recommended by Steiger and Jaeger (1977) and with correction for common Pb made using the measured $^{207}\text{Pb}/^{206}\text{Pb}$ and $^{206}\text{Pb}/^{238}\text{U}$ values following Tera and Wasserburg (1972) and as described in Compston *et al.* (1992), with appropriate model isotopic compositions after Cumming and Richards (1975). Uncertainties in the isotopic ratios and ages in the data tables (and in the error bars in the plotted data) are reported at the 1 sigma level, but final ages on pooled data are reported as weighted means with 95% confidence limits. All statistical assessments and weighted mean calculations have been performed using the program Isoplot/Ex (Ludwig, 1999).

$^{40}\text{Ar}/^{39}\text{Ar}$ methods

$^{40}\text{Ar}/^{39}\text{Ar}$ step-heating analyses were performed on mineral separates of potassium feldspar at the Research School of Earth Sciences, The Australian National University. Approximately 5 mg of each sample was wrapped in aluminium packets and placed into an aluminium irradiation canister together with interspersed aliquots of the flux monitor GA1550 (Age = 97.9 Ma; McDougall & Roksandic, 1974). Packets containing degassed potassium glass were placed at either end of the canister to monitor the ^{40}Ar production from potassium. The irradiation canister was irradiated for 504 hours in position X34 of the ANSTO, HIFAR reactor, Lucas Heights, New South Wales, Australia. The canister, which was lined with 0.2 mm Cd to absorb thermal neutrons, was inverted three times during the irradiation, which reduced neutron flux gradients to <2% along the length of the canister. After irradiation, the samples were removed from their packaging and ~1.5 mg aliquots were loaded into tin foil packets for analysis. The samples were individually dropped into a Tantalum resistance furnace and heated to progressively higher temperatures, with temperatures maintained for fifteen minutes per step. $^{40}\text{Ar}/^{39}\text{Ar}$ step-heating analyses were carried out on a VG MM12 mass spectrometer using an electron multiplier detector. Mass discrimination was monitored by analyses of standard air volumes. Correction factors for interfering reactions are as follows: $(^{36}\text{Ar}/^{37}\text{Ar})\text{Ca} = 3.50 (\pm 0.02) \times 10^{-4}$; $(^{39}\text{Ar}/^{37}\text{Ar})\text{Ca} = 7.9 (\pm 0.5) \times 10^{-4}$; $(^{40}\text{Ar}/^{39}\text{Ar})\text{K} = 0.050 (\pm 0.005)$ (Tetley *et al.*, 1980; MacDougall and Harrison, 1999). K/Ca ratios were determined from the ANU laboratory hornblende standard 77-600 and can be calculated as follows: $\text{K}/\text{Ca} = 1.90 \times ^{39}\text{Ar}/^{37}\text{Ar}$. The reported data have been corrected for system blanks, mass discrimination, reactor interferences, fluence gradients and atmospheric contamination. Errors associated with the age determinations are one sigma uncertainties and exclude errors in the J-value estimates. The error on the J-value is $\pm 0.35\%$, excluding the uncertainty in the age of GA1550 (which is ~1%). Decay constants are those of Steiger and Jaeger (1977). The $^{40}\text{Ar}/^{39}\text{Ar}$ dating technique is described in detail by MacDougall and Harrison (1999).